SPECTRA OF THE HB 21 SUPERNOVA REMNANT: EVIDENCE OF SPECTRUM FLATTENING AT THE LOW FREQUENCIES

D. Borka,[1] V. Borka Jovanović,[1] and D. Urošević[2]

RESUMEN

Utilizamos observaciones de la emisión en radiocontinuo a 1420, 820, 408, 34.5 y 22 Mhz con objeto de estimar las temperaturas de brillo medias en cinco frecuencias para el remanente de supernova HB 21. También presentamos el índice espectral medio de Hb 21. Estimamos los espectros de HB 21 mediante diagramas de temperatura media versus frecuencia, para 1420, 820, 408, 34.5 y 22 Mhz. Presentamos asimismo diagramas $T - T$ para tres pares de frecuencias, entre 1420–34.5, 1420–22, 34.5–22 MHz. Notamos que los índices espectrales son menores para frecuencias por debajo de 408 Mhz. Probablemente esto se debe a la absorción por plasma térmico a bajas frecuencias.

ABSTRACT

We use observations of the continuum radio emission at 1420, 820, 408, 34.5 and 22 MHz to estimate the mean brightness temperatures of the HB 21 supernova remnant (SNR) at five frequencies. We also present mean spectral index of HB 21. The spectra of HB 21 are estimated from mean temperatures versus frequency plots for 1420, 820, 408, 34.5 and 22 MHz. We also present $T - T$ plots of three frequency pairs: between 1420–34.5, 1420–22, 34.5–22 MHz. We notice flatter spectral indices at frequencies below 408 MHz. Probably this is due to the absorption by thermal plasma at low frequencies.

1. INTRODUCTION

The radio emission from supernova remnants (SNRs) is generally understood to be synchrotron emission from relativistic electrons moving in magnetic fields.

The HB 21 remnant is listed in Green's catalogue of Galactic supernova remnants (Green 2009a,b) as G89.0+4.7. It has mixed morphology, i.e., shell-like in radio and center-filled in the X-ray (Rho & Petre 1998). As described in Kothes et al. (2006), this is an old SNR evolving through the later stages of the Sedov phase, or early into the radiative phase (where a significant amount of the shock energy is being radiated away). Results from Byun et al. (2006) suggest that the unusual radio features and the central thermal X-ray enhancements of HB 21 might be the

result of an interaction with molecular clouds. One kind of evidence for the interaction between the SNR and the molecular cloud in HB 21 is the discovery of shocked molecular clumps by Koo et al. (2001). The center-filled, thermal X-ray emission is suggested to be caused by interaction with molecular clouds.

Flux-calibrated images and spectra of the extended remnant HB 21 in the optical range are presented in Mavromatakis, Xilouris, & Boumis (2007). Filamentary and patchy structures were detected and appear to be correlated with the radio emission.

Significant spatial variations in spectral index are found in HB 21 (Leahy 2006). He considers different physical mechanisms for spectral index changes, including a detailed consideration of ionization losses in the dense molecular gas interacting with HB 21.

One of the main goals of this paper is to provide evidence for Leahy's (2006) theoretical proposal. He suggests that if the spectra below 408 MHz show

---

[1]Vinča Institute of Nuclear Sciences, Serbia.
[2]Faculty of Mathematics, Serbia.

TABLE 1

TEMPERATURES AND BRIGHTNESSES OF HB 21 AT 1420, 820, 408, 34.5 AND 22 MHZ

Frequency (MHz)	Temperature limits $T_{\min}$, $T_{\max}$ (K)	Temperature (K)	Brightness $(10^{-22}$ W/(m^2 Hz Sr))
1420	6.0, 9.0	1.50 ± 0.05	9.26 ± 0.30
820	16.5, 26.0	4.91 ± 0.20	10.13 ± 0.40
408	87, 140	32.2 ± 1.0	16.43 ± 0.50
34.5	49000, 81000	18237 ± 700	66.60 ± 2.56
22	105000, 144000	28530 ± 500	43.34 ± 0.76

flatter spectral indices then absorption by thermal plasma would be the preferred mechanism. We show evidence for spectrum flattening at the low radio frequencies in the supernova remnant HB 21.

2. DATA AND METHOD

Measured data at five frequencies are used: 1420 (Reich & Reich 1986), 820 (Berkhuijsen 1972), 408 (Haslam et al. 1982), 34.5 (Dwarakanath & Udaya Shankar 1990) and 22 MHz (Roger et al. 1999). These surveys are available in electronic form in "Flexible Image Transport System" (FITS) data format, at the site of Max-Planck-Institut für Radioastronomie (MPIfR) near Bonn, Germany[3]. This online Survey Sampler allows users to select a region of the sky and to obtain images and data at different frequencies. The 1420-MHz Stockert survey (Reich & Reich 1986) has a resolution of 0.59°, the 820-MHz Dwingeloo survey (Berkhuijsen 1972) 1.2°, the 408-MHz all-sky survey (Haslam et al. 1982) 0.85°, the 34.5-MHz Gauribidanur survey (Dwarakanath & Udaya Shankar 1990) 0.7° and 22 MHz (Roger et al. 1999) 1.7°. The corresponding observations are given at the following rates (measured data) for both l and b: 1/4° at 1420 MHz, 1/2° at 820 MHz, 1/3° at 408 MHz, 1/5° at 34.5 MHz and 1/4° at 22 MHz. The effective sensitivities are about 50 mK $T_{\rm b}$ ($T_{\rm b}$ is for an average brightness temperature), 0.20 K, 1.0 K, about 700 K and about 500 K, respectively. We extracted observed brightness temperatures from these data and then using programs in C and FORTRAN, obtained the results shown in this paper.

The area of HB 21 SNR is enclosed with brightness temperature contours. The maps of a region in HB 21 SNR, in new Galactic coordinates (l, b), with contours of the brightness temperatures $T_{\rm b}$ are plotted in Figures 1–5. The contour lines correspond to

the brightness temperatures: minimum, maximum and nine contours in between. The space between minimum and maximum contours defines the HB 21 SNR. The Galactic longitude and latitude intervals for HB 21 SNR are the following: $l = [90°, 87.5°]$, $b = [3.5°, 6°]$. We used the same method of calculation as given in Borka (2007) for Galactic radio loops I–VI, Borka, Milogradov-Turin, & Urošević (2008) for Loops V and VI, Borka Jovanović & Urošević (2009) for the Monoceros loop and in Borka Jovanović & Urošević (2011) for the Cygnus loop.

The mean temperatures and surface brightnesses of this SNR are computed using data taken from radio-continuum surveys at 1420, 820, 408, 34.5 and 22 MHz. The areas over which an average brightness temperature is determined at each of the five frequencies are taken to be as similar as possible within the limits of measurement accuracy. However, some differences between these areas still remain and we think that the major causes of differing borders between the five frequencies are measurement accuracy and small random and systematic errors in the data. The surface brightness of SNR must be above the sensitivity limit of the observations and must be clearly distinguishable from the Galactic background emission (Green 1991). In order to evaluate brightness temperatures over the SNR we took into account background radiation (see Webster 1974). Borders enclosing the SNR are defined to separate the SNR from the background.

We have subtracted the background radiation, in order to derive the mean brightness temperature of the SNR alone. $T_{\min}$ in Table 1 denotes the lower temperature limit between the background and the SNR, and $T_{\max}$ the upper temperature of the SNR. We used all measured values inside the corresponding regions of l and b, to calculate the brightness temperature of a SNR including the background. The mean brightness temperature for the SNR is found
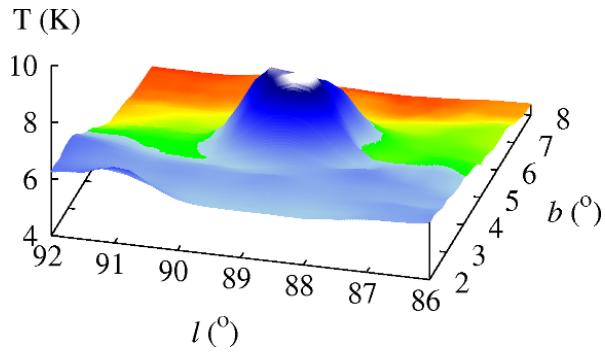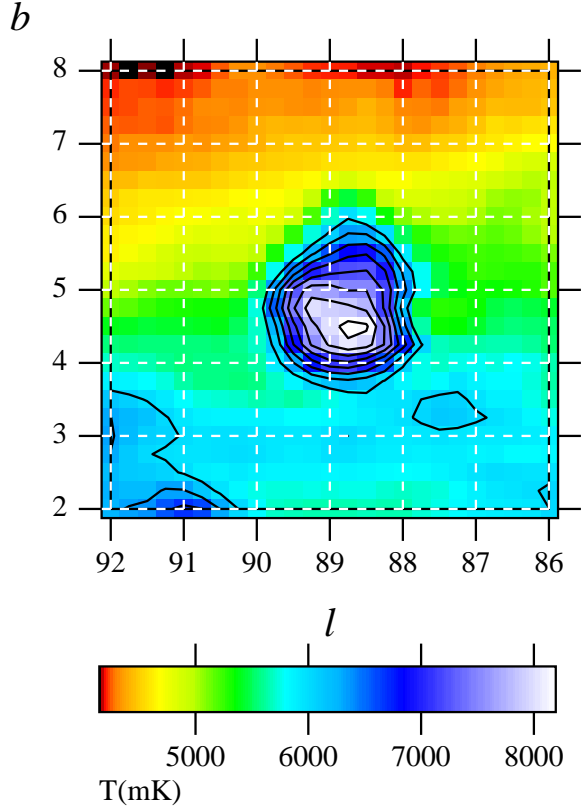
---

[3] http://www.mpifr-bonn.mpg.de/survey.html.

Fig. 1. Top: The radio map of HB 21 SNR at 1420 MHz with contours of brightness temperature. This SNR has position: $l = [90.°, 87.5°]$; $b = [3.5°, 6°]$, in new Galactic coordinates (l, b). The eleven contours plotted represent the temperatures T_{min} and T_{max} from Table 1 and nine contours in between. The contour interval is 0.3 K T_b, starting from the lowest temperature of 6 K up to 9 K. The corresponding temperature scale is given. Bottom: the 1420 MHz area map of Cygnus. The color figure can be viewed online.

by subtracting the mean value of background brightness temperature from the mean value of the brightness temperature over the area of the SNR.
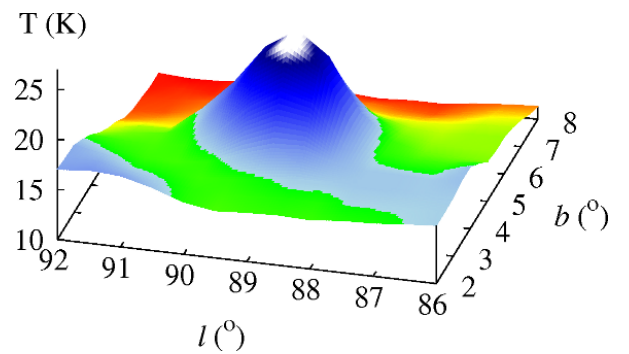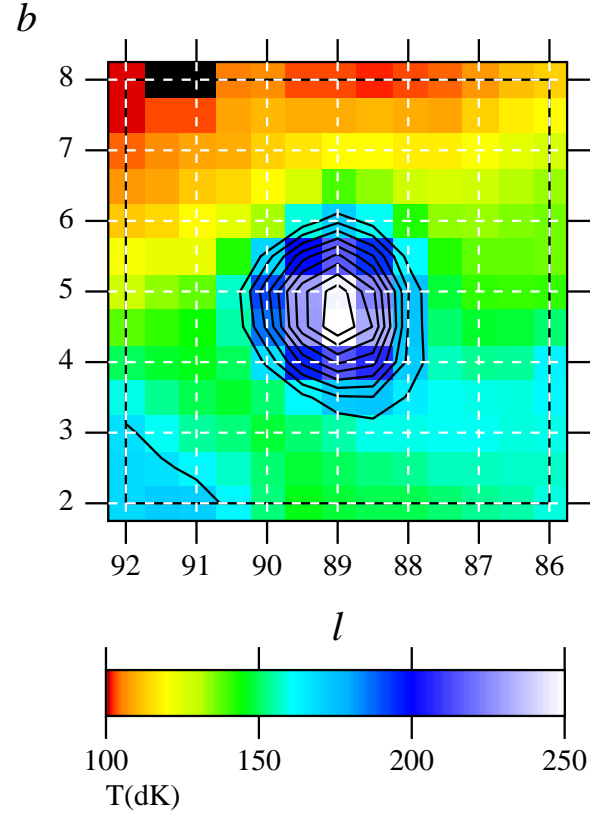
Fig. 2. The same as Figure 1, but for 820 MHz. The contour interval is 0.95 K T_b, starting from the lowest temperature of 16.5 K up to 26 K. The color figure can be viewed online.

After deriving the mean brightness temperatures T_ν, we derived surface brightnesses Σ_ν by means of:

$$\Sigma_\nu = \left(2k\nu^2/c^2\right) T_\nu . \qquad (1)$$

where k is Boltzmann constant and c the speed of light. Results are given in Table 1.

3. DISCUSSION AND RESULTS

The results for the temperature limits are given in Table 1. T_{min}, given in the second column of Ta-
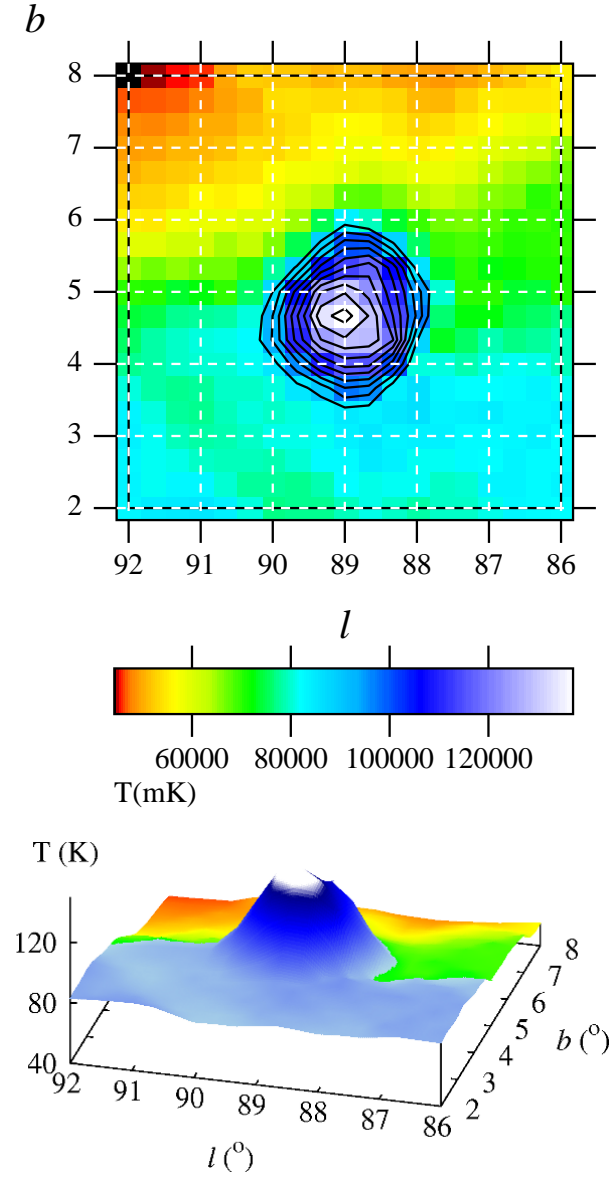
Fig. 3. The same as Figure 1, but for 408 MHz. The contour interval is 5.3 K T_b, starting from the lowest temperature of 87 K up to 140 K. The color figure can be viewed online.

Fig. 4. The same as Figure 1, but for 34.5 MHz. The contour interval is 3200 K T_b, starting from the lowest temperature of 49000 K up to 81000 K. The color figure can be viewed online.

ble 1, is the lower temperature limit, while T_{max} is the upper temperature limit given in the third column of Table 1. There are some other sources near the SNR and they do not affect the calculation. These temperature limits enable us to distinguish the SNR from the background and also from external sources. Then we derived the temperatures and the surface brightnesses using equation (1) for each frequency. These results are given in the forth and fifth columns of Table 1, respectively. Brightnesses
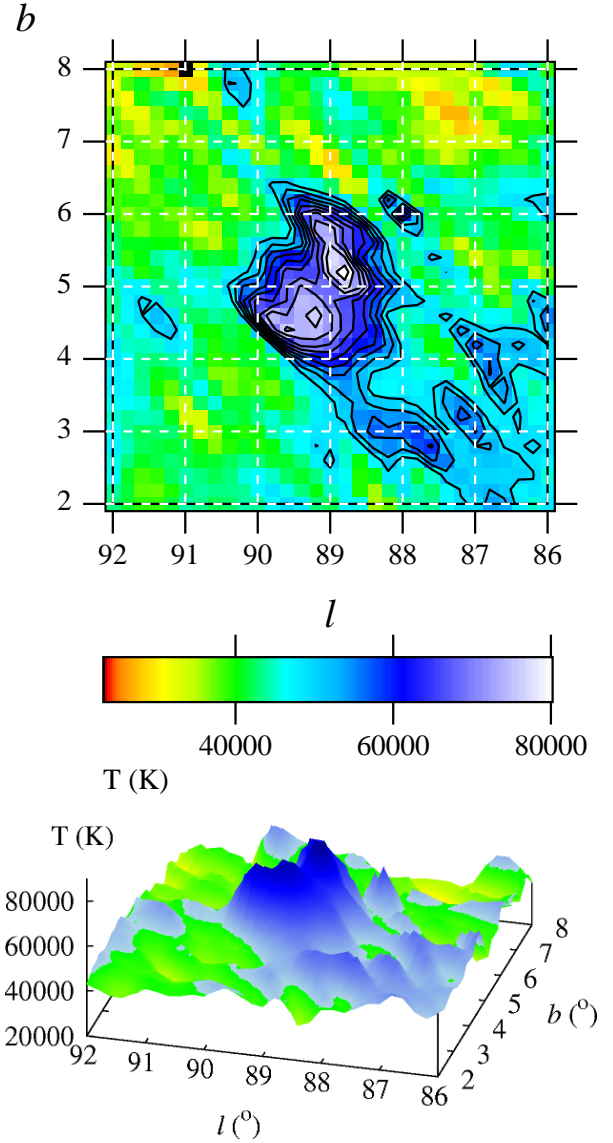
of HB 21 reduced to 1000 MHz, using spectral index $\alpha = 0.45 \pm 0.07$ are given in Table 2.

The radio map of HB 21 SNR at 1420 MHz with contours of brightness temperature is given in Figure 1. This SNR has position: $l = [90.0°, 87.5°]$; $b = [3.5°, 6°]$, in new Galactic coordinates (l, b). The eleven contours plotted represent the temperatures T_{min} and T_{max} from Table 1 and nine contours in between. The contour interval is 0.3 K T_b, starting from the lowest temperature of 6 K up to 9 K. Also, the corresponding temperature scale is given.
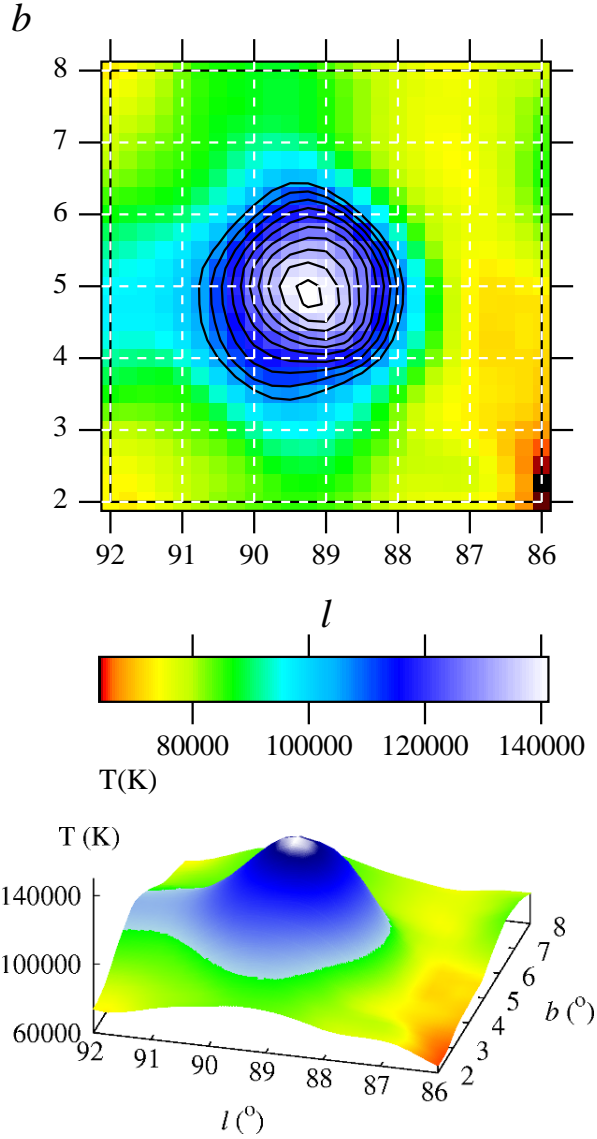
Fig. 5. The same as Figure 1, but for 22 MHz. The contour interval is 3900 K T_b, starting from the lowest temperature of 105000 K up to 144000 K. The color figure can be viewed online.

In Figure 2 is presented the radio map of HB 21 SNR at 820 MHz with contours of brightness temperature. The contour interval is 0.95 K T_b, starting from the lowest temperature of 16.5 K up to 26 K. The radio map of HB 21 SNR at 408 MHz with contours of brightness temperature is given in Figure 3. The contour interval is 5.3 K T_b, starting from the lowest temperature of 87 K up to 140 K. In Figure 4 is presented the radio map of HB 21 SNR at 34.5 MHz with contours of brightness temperature. The contour interval is 3200 K T_b, starting from the lowest temperature of 49000 K up to 81000 K. The

TABLE 2

BRIGHTNESSES OF HB 21 REDUCED TO 1000 MHZ, USING A SPECTRAL INDEX $\alpha = 0.45 \pm 0.07$

Frequency (MHz)	Brightness reduced to 1000 MHz (10^{-22} W/m^{-2} Hz^{-1} Sr^{-1})
1420	10.83 ± 0.64
820	9.27 ± 0.24
408	11.01 ± 0.38
34.5	14.80 ± 3.10
22	7.88 ± 2.08

radio map of HB 21 SNR at 22 MHz with contours of brightness temperature is given in Figure 5. The contour interval is 3900 K T_b, starting from the lowest temperature of 105000 K up to 144000 K. The corresponding temperature scale is given for brightness temperatures of HB 21 at 1420, 820, 408, 34.5 and 22 MHz in Figures 1–5, respectively.

3.1. *Spectrum*

The dominant emission mechanism from Galactic supernova remnants (SNRs) at radio frequencies is synchrotron emission. However, some SNRs, observations over a very broad range of radio frequencies reveal a curvature in the spectra of these sources (Leahy 2006; Tian & Leahy 2005). The detection of thermal emission at radio frequencies from Galactic SNRs shows whether or not these sources are interacting with adjacent molecular clouds. It might also be useful for estimating the ambient density near SNRs using radio continuum data (Urošević, Pannuti, & Leahy 2007). The presence of a significant amount of thermal emission will produce a curvature in the observed radio spectrum of the SNR, particularly for frequencies of 1 GHz and greater (Urošević et al. 2007).

The radio continuum spectrum of HB 21 SNR (temperature vs frequency), is presented in Figure 6. Spectra for five measurements at 22, 34.5, 408, 820 and 1420 MHz are represented by a solid line, the spectrum obtained from the three frequencies 408, 820 and 1420 MHz is shown by a dashed line, and the spectrum obtained from the two lowest frequencies 22 and 34.5 MHz is shown by a dash-dot line. The spectrum was generated using mean temperatures at five different frequencies (see Figure 6). The brightness temperature spectral index is defined by equation (2). All five frequencies 1420, 820, 408, 34.5 and 22 MHz, from a linear fit, give $\alpha_5 = 0.45 \pm 0.07$.
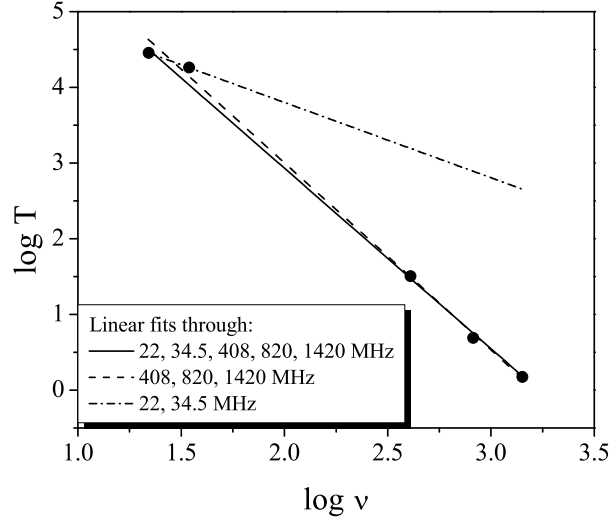
Fig. 6. The radio continuum spectrum of the HB 21 SNR: temperature versus frequency. The spectrum for five measurements at 22, 34.5, 408, 820 and 1420 MHz is given by a solid line, the spectrum obtained from the three frequencies 408, 820 and 1420 MHz is given by a dashed line, and the spectrum obtained from the two lowest frequencies 22 and 34.5 MHz is given by a dash-dot line.

Frequencies 34.5 and 22 MHz lie on the very low ends of the spectrum, as presented in Figure 6, and we analyze them separately. A derived value $\alpha_2 = -1.01$ (from two frequencies), suggests possible thermal absorption at the very low end of the spectrum.

The curved spectrum of the third order of HB 21, obtained from the five frequencies is presented in Figure 7. The spectra obtained show that a curvature (Baars, Mezger, & Wendker 1965; Milogradov-Turin & Nikolić 1995) is present in the radio spectrum at low frequencies, see Figure 7. In the papers Baars et al. (1965), Milogradov-Turin & Nikolić (1995) the spectra are represented by a second order polynomial fit. For our spectra we used a polynomial fit of third order. This third order polynomial regression line fits properly the temperature versus frequency for five measurements, at 22, 34.5, 408, 820 and 1420 MHz. The parameters of the third order polynomial fit are: $a = -0.582641 \pm 0.1809$ (31.04%), $b = 9.38084 \pm 0.2556$ (2.725%), $c = -5.15063 \pm 0.1133$ (2.201%), $d = 0.714124 \pm 0.01609$ (2.254%).

We are using two equations:

$$T = K\nu^{-\beta} = K\nu^{-(\alpha+2)}, \qquad (2)$$

$$\log T = a + b \log \nu + c \log^2 \nu + d \log^3 \nu. \qquad (3)$$

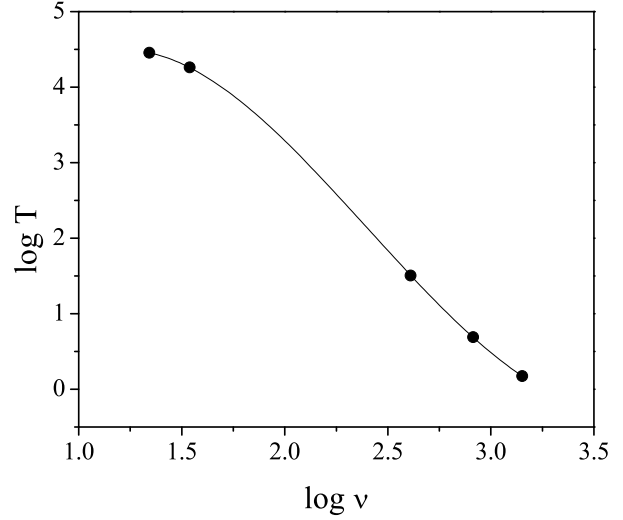Equation (2) represents the dependence between brightness temperature, frequency as well as bright-

Fig. 7. The curved spectrum of the third order of HB 21, obtained from the five frequencies.

ness temperature spectral index β, ($\beta = \alpha + 2$, where α represents the flux density spectral index) and K is a constant. Equation (3) represents the third order polynomial fit and tells us about the dependence T of ν. Using equations (2) and (3) and after taking a log of both sides of equations and deriving both sides with respect to ν we obtain the expression:

$$\alpha^c(\nu) = -(b + 2c \log \nu + 3d \log^2 \nu) - 2, \qquad (4)$$

where the index c denotes curved spectrum.

We want to stress that the same procedure can be used if the spectrum is given in terms of flux density because the relation (1) holds between brightness Σ_ν and brightness temperature T_ν and between flux density S_ν and brightness Σ_ν the relation holds:

$$S_\nu = \Sigma_\nu \, \Omega, \qquad (5)$$

where Ω is the solid angle.

The new equation will be the same as equation (3), but with different coefficients

$$\log S_\nu = a' + b' \log \nu + c' \log^2 \nu + d' \log^3 \nu. \qquad (6)$$

We choose the spectrum given in terms of T_b because our original data involve T_b, not the flux density.

Using these parameters and equation (4) we can derive the dependence of the spectral index on frequency along the entire frequency range from 22 to 1420 MHz. Variations of the spectral index $\alpha^c(\nu)$ with frequency in the case of HB 21 are presented in Figure 8. The spectral index $\alpha^c(\nu)$ is obtained
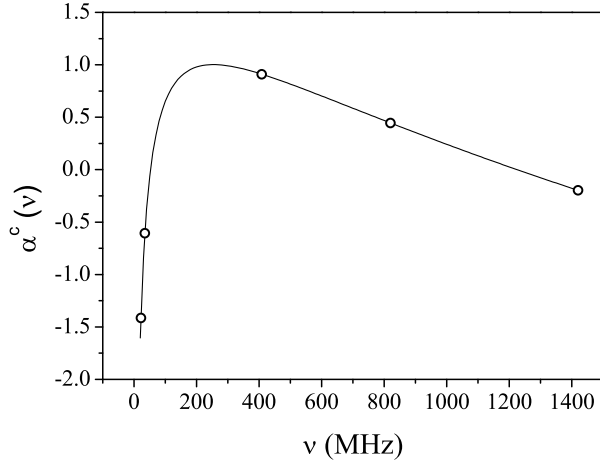
Fig. 8. Variations of spectral index $\alpha^c(\nu)$ with frequency in the case of HB 21. The spectral index $\alpha^c(\nu)$ is obtained from the third order polynomial fit presented in Figure 7. Open circles represent values of spectral indices $\alpha^c(\nu)$ at the five observed frequencies.

from the third order polynomial fit presented in Figure 7. Open circles represent values of the spectral indices at the five observed frequencies. We notice flatter spectral indices at low frequencies, below about 200 MHz. Probably this is due to the thermal mechanism at frequencies below about 200 MHz or below the observed frequency of 408 MHz. Absorption by thermal plasma is probably the preferred mechanism in the low frequency range of the spectra, as proposed by Leahy (2006).

From the curved spectrum, we can also calculate the spectral index α^c using equation (4). In this case α is function of ν, and therefore for the mean α we use:

$$\bar{\alpha}^c = \frac{1}{\nu_{\max} - \nu_{\min}} \int_{\nu_{\min}}^{\nu_{\max}} \alpha^c(\nu) d\nu \,, \qquad (7)$$

where $\nu_{\min} = 22$ MHz and $\nu_{\max} = 1420$ MHz. Using equations (4) and (7) we obtain $\bar{\alpha}^c_{22-1420} = 0.46$. When we insert $\nu_{\min} = 22$ MHz and $\nu_{\max} = 34.5$ MHz the result is $\bar{\alpha}^c_{22-34.5} = -0.97$.

Since we deal with mean brightness temperature, we lose the information about index variations because for each frequency we have only one average value for the brightness temperature. Using equation (2) we obtain a connection between brightness temperature and spectral index α. We plot the dependence $\log T$ vs $\log \nu$. The dependence $\log \nu$ between 408, 820 and 1420 MHz can be nicely represented by a straight line. Leahy (2006) obtained a mean spectral index $\alpha = 0.45$ using observations

at 408 and 1420 MHz, and from our Figure 8 using only points at 408 and 1420 MHz we obtain $\alpha = 0.47$ which is in excellent agreement with Leahy's value. But if we take into account the low frequencies at 22 and 34.5 MHz we find that now the dependence $\log T$ vs $\log \nu$ is nicely represented by the polynomial fit of third order.

This indicates that the spectrum of HB 21 is a combination of synchrotron and thermal components. The presence of the additional component in the radio spectrum of HB 21 suggests that HB 21 is probably interacting with an adjacent molecular cloud.

3.2. $T - T$ plot

The measured data have different resolutions for different frequencies. In order to obtain $T - T$ plots the data are retabulated. We convolved data at 1420, 34.5 and 22 MHz to $0.25° \times 0.25°$ resolution. Sampling rates of the 820 MHz and 408 MHz surveys are much more crude and we did not take them into account. Then, for each frequency pair we used only the common points [with the same (l, b)] which belong to the loop area at both frequencies. In that way we reduced loop area to the same area for different frequencies. The obtained $T-T$ plots for three pairs of frequencies enabled us to calculate the spectral indices. We calculated two α values for each of these tree frequency pairs: between 1420–34.5, 1420–22, 34.5–22 MHz. For each of the tree frequency pairs, by interchanging the dependent and independent variables we have obtained two α values for each pair and the mean value of these fit results is adopted as the radio spectral index, as suggested in Uyaniker et al. (2004). Regarding the two pairs of frequencies 1420–34.5, 1420–22 the average value of the spectral index from the $T - T$ plot is $<\alpha_{\mathrm{TT}}>_{1420-22,1420-34.5} = 0.47 \pm 0.29$. Regarding the lowest pair of frequencies 34.5–22, the average value of the spectral index from the $T - T$ plot is $<\alpha_{\mathrm{TT}}>_{34.5-22} = -0.82 \pm 0.82$.

It can be noticed that this value agrees well with the corresponding value obtained from the spectrum, as expected (see Uyaniker et al. 2004).

Leahy (2006) determined in HB 21 SNR a mean spectral index of 0.45. Our mean spectral index is in agreement with Leahy. He found significant spectral index variations and concluded that thermal absorption was the preferred mechanism (Leahy 2006). He concluded that if thermal plasma absorption or ionization losses are the correct mechanism, frequencies below 408 MHz should show flatter spectral indices and one should be able to distinguish which mechanism is working, since ionization losses will have

no indices flatter than 0.25 (Leahy 2006). We obtained spectral indices flatter than 0.25 for the HB 21 SNR in the low frequency domain, and we can expect that thermal plasma absorption is responsible for the spectral flattening at the lowest radio frequencies.

4. CONCLUSIONS

We use observations of the continuum radio emission at 1420, 820, 408, 34.5 and 22 MHz to estimate the mean brightness temperatures and surface brightnesses of the HB 21 SNR. The sensitivity of the brightness temperatures is: 50 mK for 1420 MHz, 0.2 K for 820 MHz, 1.0 K for 408 MHz, about 700 K T_b for 34.5 MHz and about 500 K T_b for 22 MHz.

We present the radio continuum spectrum of the HB 21 SNR using average brightness temperatures at five frequencies. As can be seen from Figure 6, the given linear fit provides a reliable spectral index. Our analysis indicates that significant spectral variations of the spectral index for different frequencies are found in HB 21. We noticed flatter spectral indices at frequencies below 408 MHz, as proposed by Leahy (2006).

This indicates that the spectrum of HB 21 is a combination of synchrotron and thermal components. The presence of the additional component in the radio spectrum of HB 21 suggests that this SNR is interacting with an adjacent molecular cloud.

In Leahy (2006), observations of the SNR HB 21 are presented at 408 and 1420 MHz. He considered different physical mechanisms for the spectral index variations. He concluded that if the spectra below 408 MHz show flatter spectral indices then absorption by thermal plasma is the preferred mechanism. Our obtained spectra at 5 frequencies leads to a similar conclusion.

We note an obvious flattening of the spectral indices. In future work one might investigate a broader frequency range. Probably, thermal emission at higher frequencies will produce a curvature in the radio spectrum of the HB 21 SNR, particularly for frequencies higher then 1 GHz (Urošević et al. 2007).

REFERENCES

Baars, J. W. M., Mezger, P. G., & Wendker, H. 1965, ApJ, 142, 122
Berkhuijsen, E. M. 1972, A&AS, 5, 263
Borka, V. 2007, MNRAS, 376, 634
Borka, V., Milogradov-Turin, J., & Urošević, D. 2008, Astron. Nachr., 329, 397
Borka Jovanović, V., & Urošević, D. 2009, Astron. Nachr., 330, 741
_____. 2011, RevMexAA, 47, 159
Byun, D.-Y., Koo, B.-C., Tatematsu, K., & Sunada, K. 2006, ApJ, 637, 283
Dwarakanath, K. S., & Udaya Shankar, N. 1990, J. Astrophys. Astron., 11, 323
Green, D. A. 1991, PASP, 103, 209
_____. 2009a, A Catalogue of Galactic Supernova Remnants (2009 March version), Astrophysics Group, Cavendish Laboratory, Cambridge, UK (available at http://www.mrao.cam.ac.uk/surveys/snrs/)
_____. 2009b, Bull. Astron. Soc. India, 37, 45
Haslam, C. G. T., Salter, C. J., Stoffel, H., & Wilson, W. E. 1982, A&AS, 47, 1
Koo, B.-C., Rho, J., Reach, W. T., Jung, J., & Mangum, J. G. 2001, ApJ, 552, 175
Kothes, R., Fedotov, K., Foster, T. J., & Uyaniker, B. 2006, A&A, 457, 1081
Leahy, D. A. 2006, ApJ, 647, 1125
Mavromatakis, F., Xilouris, E. M., & Boumis, P. 2007, A&A, 461, 991
Milogradov-Turin, J., & Nikolić, S. 1995, Bull. Astron. Belgrade, 152, 11
Reich, P., & Reich, W. 1986, A&AS, 63, 205
Rho, J., & Petre, R. 1998, ApJ, 503, L167
Roger, R. S., Costain, C. H., Landecker, T. L., & Swerdlyk, C. M. 1999, A&AS, 137, 7
Tian, W., & Leahy, D. 2005, A&A, 436, 187
Urošević, D., Pannuti, T. G., & Leahy, D. 2007, ApJ, 655, L41
Uyaniker, B., Reich, W., Yar, A., & Fürst, E. 2004, A&A, 426, 909
Webster, A. S. 1974, MNRAS, 166, 355

D. Borka and V. Borka Jovanović: Atomic Physics Laboratory (040), Vinča Institute of Nuclear Sciences, University of Belgrade, P.O. Box 522, 11001 Belgrade, Serbia (dusborka, vborka@vinca.rs).
D. Urošević: Department of Astronomy, Faculty of Mathematics, University of Belgrade, Studentski trg 16, 11000 Belgrade, Serbia (dejanu@math.rs).